[CANCER RESEARCH 61, 3894–3901, May 15, 2001]

Ionizing Radiation-induced, Mitochondria-dependent Generation of Reactive Oxygen/Nitrogen[1]

J. Kevin Leach, Glenn Van Tuyle, Peck-Sun Lin, Rupert Schmidt-Ullrich, and Ross B. Mikkelsen[2]

Departments of Radiation Oncology [J. K. L., P-S. L., R. S-U., R. B. M.] and Biochemistry [G. V. T.], Virginia Commonwealth University, Richmond, Virginia 23298

ABSTRACT

Transient generation of reactive oxygen or nitrogen (ROS/RNS), detected with dihydrodichlorofluoroscein by fluorescence microscopy, occurs within minutes of exposing cells to ionizing radiation. In the 1–10 Gy dose range, the amount of ROS/RNS produced/cell is constant, but the percentage of producing cells increases with dose (20 to 80%). Reversible depolarization of the mitochondrial membrane potential ($\Delta\Psi$) and decrease in fluorescence of a mitochondria-entrapped dye, calcein, are observed coincidentally. Radiation-induced ROS/RNS, $\Delta\Psi$ depolarization, and calcein fluorescence decrease are inhibited by the mitochondrial permeability transition inhibitor, cyclosporin A, but not the structural analogue, cyclosporin H. Radiation-stimulated ROS/RNS is also inhibited by overexpressing the Ca^{2+}-binding protein, calbindin 28K, or treating cells with an intracellular Ca^{2+} chelator. Radiation-induced ROS/RNS is observed in several cell types with the exception of ρ^o cells deficient in mitochondrial electron transport. ρ^o cells show neither radiation-induced ROS/RNS production nor $\Delta\Psi$ depolarization. We propose that radiation damage in a few mitochondria is transmitted via a reversible, Ca^{2+}-dependent mitochondrial permeability transition to adjacent mitochondria with resulting enhanced ROS/RNS generation. Measurements of radiation-induced mitogen-activated protein kinase activity indicate that this sensing/amplification mechanism is necessary for activation of some cytoplasmic signaling pathways by low doses of radiation.

INTRODUCTION

Extensive progress has been made in the understanding of mechanisms by which ionizing radiation-induced DNA damage is sensed within the nucleus and translated into the activation of cell cycle checkpoints and DNA damage repair processes (1–5). Less is known about the consequences of cytoplasmic irradiation and whether initial cytoplasmic events impinge on nuclear processes. Components of cytoplasmic signal transduction pathways that are rapidly activated after irradiation include Tyr kinases such as the epidermal growth factor receptor, cytoplasmic Ca^{2+} homeostasis mechanisms, protein kinase C, MAP[3] kinases, JUN kinases, and ceramide production (6–12). These cytoplasmic pathways are integrated into the growth regulatory networks of cells, and the relative balance of the proliferative and antiproliferative signals activated by radiation may determine cell fate (1).

An important question is how a few primary ionization events (approximately 2000/Gy/cell) are amplified sufficiently to account for the relatively rapid and robust activation of these cytoplasmic signal transduction pathways (1, 5). This issue was raised previously (5) in a comparison between UV and ionizing radiation in terms of potential mechanisms by which these two types of radiation stimulate Tyr kinase activities. Theoretical calculations indicated that for UV radiation the amount of damage produced in non-DNA molecules is sufficient to account for induction of cytoplasmic signal transduction pathways. At equivalent stimulating doses, this contrasts with the low yield and lack of specificity in the damage produced by ionizing radiation. The major ROS of the primary ionization event, the hydroxyl radical, is also short-lived and can only diffuse approximately 4 nm before reacting (13). Secondary ROS products can potentially amplify the initial ionization event, but theoretical calculations indicate that the yields of hydrogen peroxide or superoxide anion generated as a consequence of a primary ionization event are lower by orders of magnitude than that produced by normal cellular metabolism (5).

Evidence for an extranuclear amplification mechanism involving ROS (or RNS) has come from studies in which cellular ROS/RNS levels after radiation exposure were measured with a fluorescent dye, dihydro-DCF (14–16). Exposing cells to either α-particles or γ-radiation significantly enhanced cellular ROS/RNS levels above that attributable to normal cell metabolism. With α-particle radiation, experiments with dihydroethidium, a fluorescent dye sensitive to superoxide anion, confirmed radiation-induced ROS generation (14). Measurements of ROS/RNS in both studies were obtained at relatively late times (>15 min) after irradiation. For this reason, it is difficult to judge whether the increase in ROS/RNS after irradiation reflected the activation of an early signal transduction pathway or was a consequence of enhanced ROS/RNS production by a small population of cells undergoing apoptosis (17). A possible source of cellular ROS stimulated by radiation was not identified.

In the present investigation, we reasoned that if ROS/RNS generation induced by ionizing radiation represents a cytoplasmic amplification mechanism, it should be observed at much earlier times. For these experiments, digitized fluorescence microscopy with a ^{90}Sr-radiation source mounted on the microscope permitted rapid measurements during and after irradiation. We also reasoned that a potential source for the ROS/RNS would be the mitochondria because they are the major cellular source of ROS in most cells, and the total cellular mitochondrial volume (4–25% depending on the cell) represents a fairly substantial cellular target volume. Hence, we evaluated whether radiation-induced changes in mitochondrial permeability is one mechanism by which an oxidative event in one mitochondrion can be transmitted throughout the mitochondrial population of a given cell (18–21). Our findings indicate that ionizing radiation induces a reversible mitochondrial permeability transition and agents that inhibit this transition block radiation-induced ROS/RNS generation activation of downstream signal transduction.

MATERIALS AND METHODS

Cells and Cell Culture. The A431 squamous carcinoma, MDA-MB-231 breast carcinoma, DU145 and PC-3 prostate carcinomas, and CHO cell lines were purchased from American Type Culture Collection (Gaithersburg, MD). MCF-7 breast carcinoma cells were provided by Dr. Marc Lipmann (Georgetown University, Washington, D.C.). Dr. Michael King (Thomas Jefferson University, Philadelphia, PA) provided the osteosarcoma 143BTK$^-$ ρ^o and ρ^+

Received 11/21/00; accepted 3/16/01.

The costs of publication of this article were defrayed in part by the payment of page charges. This article must therefore be hereby marked *advertisement* in accordance with 18 U.S.C. Section 1734 solely to indicate this fact.

[1] Supported by United States Public Health Service Grants CA 65896 and CA72955, developmental funds from the Massey Cancer Center, and a generous gift from Tanya Gordon.

[2] To whom requests for reprints should be addressed, at Department of Radiation Oncology, Virginia Commonwealth University, Richmond, VA 23298. Phone: (804) 628-0857; Fax: (804) 828-6042; E-mail: rmikkels@vcu.edu.

[3] The abbreviations used are: MAP, mitogen-activated protein; BA, bongkrekic acid; BAPTA/AM, 1,2-bis(2-aminophenoxy)ethane-N,N,N′,N′-tetraacetic acid; CsA, cyclosporin A; CsH, cyclosporin H; DCF dichlorofluoroscein; FCCP, carbonyl cyanide *p*-trifluoromethoxy-phenylhydrazone; RNS, reactive nitrogen species; ROS, reactive oxygen species; TMRE, tetramethylrhodamine ethyl ester.

cells (22). All of the cells were grown in RPMI 1640 plus 5% FCS and antibiotics. The culture medium of osteosarcoma cells also contained 50 μg/ml uridine. CHO cells were transfected with the LipofectAMINE PLUS kit according to the manufacturer's directions (Life Technologies, Inc.).

Reagents and their suppliers were: fluorescent probes, BAPT/AM, and CsA (Molecular Probes, Eugene, OR); CsH (Novartis, Vienna, Austria); and BA (Calbiochem, San Diego, CA). The BSR and BSR-CaBD plasmids for expression of calbindin 28K (23) were kindly provided by Dr. Sylvia Christakos (New Jersey Medical School, Newark, NJ).

ROS/RNS Production. DCF, which is nonfluorescent in its dihydro form but upon reaction with ROS/RNS becomes highly fluorescent, was used as described in previous studies (14–16, 24). Dihydro-DCF is sensitive to oxidation by hydroxyl radicals and peroxynitrite directly and hydrogen peroxide in the presence of a peroxidase (16, 24). For this reason, we refer to both ROS and RNS in describing the experimental results obtained with DCF. Preliminary studies demonstrated that the membrane permeant acetooxymethyl ester derivative of dihydro-DCF was better retained by the cells than the diacetate derivative.

The spectroscopic properties of DCF do not permit ratiometric measurements that provide internal controls for dye leakage and cell volume sampled. The approach used in the present study to facilitate comparisons between cells in terms of relative changes in DCF fluorescence involved coloading with a radiation-insensitive dye and following DCF fluorescence relative to the fluorescence of this dye. As a radiation-insensitive dye, fura-2 excited at its isobestic, Ca^{2+}-independent excitation wavelength was used (6). As shown in Fig. 1, fura-2 fluorescence excited at 360 nm was constant over the time period examined and not affected by radiation. This dual labeling approach permitted quantitative comparisons between cells within a single cell preparation. However, differences in dye loading from one cell preparation to another did not allow for quantitative comparisons between cell preparations.

The dye-loading conditions were as follows. Cells grown on round glass coverslips were equilibrated with the acetooxymethyl esters of dihydro-DCF (5 μM) and fura-2 (2 μM) in phenol red-free RPMI 1640 supplemented with 10 mM HEPES (pH 7.4) for 30 min at room temperature. Cells were rinsed with the same buffer without dye and incubated for an additional 30 min before mounting in a perfusion chamber and microscopic analysis. Equivalent results were obtained if cells were also maintained in PBS containing 5 mM glucose, 1 mM $MgCl_2$, and 1 mM $CaCl_2$. DCF fluorescence was monitored with excitation at 490 nm and emission at 530 nm. Fura-2 fluorescence was simultaneously monitored at an excitation wavelength of 360 nm with emission at 530 nm (6).

A digitized video-intensified imaging analysis system described previously (6) with a DAGE-MTI silicone-intensified video camera was used for analysis. The computer coordinates excitation filter movement with image capture and calculates intensity ratios in the DCF/fura-2 experiments. Individual cells and a background area were delimited with the computer mouse using the fura-2 or brightfield images. The measured fluorescence signal was the average pixel value for the entire cell minus the average background pixel value. Because dihydro-DCF is readily photooxidized, a 1.0 *A* neutral density filter was used with the 490-nm excitation filter to minimize photooxidation. Measurements were made every 20–30 s with a 0.5-s acquisition time. A ^{90}Sr-eye applicator mounted on the condensing lens holder of an inverted Nikon Diaphot microscope was lowered to a predetermined distance to initiate irradiation at a dose rate of 6 Gy/min (6). Radiation exposure was terminated by removal of the source at designated times to give the indicated total dose.

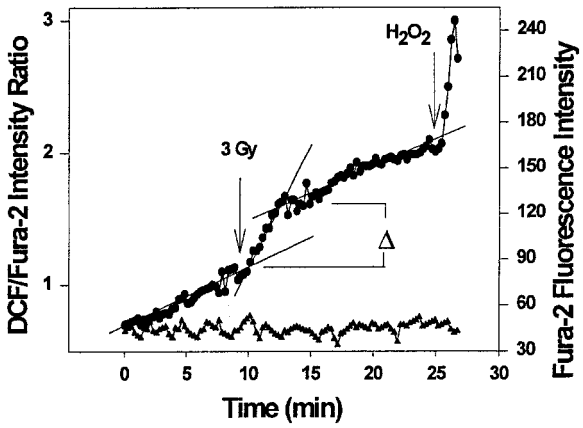

Fig. 1. Ionizing radiation stimulates ROS/RNS generation in A431 cells. Dye loading and fluorescence measurements are described in the text. The results are shown for a representative cell responding to radiation with an increase in DCF fluorescence normalized to fura-2 fluorescence after exposure to 3 Gy. The indicated slopes were calculated by linear regression using SigmaPlot software. The magnitude of the response, Δ, was calculated from the slopes as shown in the figure.

For bulk measurements of ROS/RNS, cells were plated in a 96-well plate at 10^4 cells/well 24 h before irradiation. Cells were loaded with dihydro-DCF as described above and irradiated at a dose rate of 2.1 Gy/min with a ^{60}Co source. Half of the plate was shielded with a lead brick for the control, nonirradiated cells. Control experiments with dye in the wells without cells indicated that radiation alone did not oxidize dihydro-DCF. Fluorescence measurements were obtained with a Packard Fluorocount plate reader.

Mitochondrial $\Delta\Psi$ Measurements. Mitochondrial $\Delta\Psi$ was measured with the fluorescent cation, TMRE. Cells on coverslips were equilibrated for 10 min with 100 nM TMRE in phenol red-free, RPMI 1640 containing 10 mM HEPES (20). Imaging was as described for DCF but with the Nikon rhodamine filter set.

Mitochondrial Calcein Release. Cells were coloaded with 5 μM acetooxymethyl ester of calcein and 1 mM $CoCl_2$ for 30 min at 37°C in phenol red-free, HEPES-buffered RPMI 1640 (25–28). Before image analysis, cells were washed once in this medium without dye and $CoCl_2$. Imaging was as described above with the Nikon fluorescein filter set.

MAP Kinase Activity. Cells at approximately 80% confluency in 60-mm dishes were irradiated and at the given times washed twice with ice-cold PBS and then snap frozen on dry ice. Cell lysates were prepared, and MAP kinase activity was measured by an immune complex assay with myelin basic protein as substrate, as described previously (29).

RESULTS

Ionizing Radiation Stimulates Cellular ROS/RNS Production. To measure ROS/RNS, we used dihydro-DCF, which becomes fluorescent upon oxidation by ROS/RNS. This dye has been extensively used in studies on cellular ROS/RNS generation (14–16, 24). Fig. 1 shows representative recordings from a single A431 cell that responded to a radiation exposure with increased DCF fluorescence. The lower tracing is that for fura-2 and is constant during the time course of the experiment as expected for excitation at 360 nm, the isobestic and Ca^{2+}-insensitive wavelength of fura-2. The upper tracing is for DCF fluorescence normalized to fura-2 fluorescence. Fura-2 fluorescence excited at this wavelength permits normalization of DCF fluorescence values with respect to the cell volume sampled. At the end of each experiment, 100 μM hydrogen peroxide is added as an internal control. Before irradiation, there is a continuous increase in DCF fluorescence attributable mostly to ROS generated from normal mitochondrial respiration. This background ROS/RNS generation is sensitive to mitochondrial poisons such as rotenone and much reduced in mitochondrial electron transport-deficient ρ^o cells (see results below in Fig. 3). After a stable baseline recording is obtained, the ^{90}Sr source is lowered to a given distance above the cells, initiating the radiation exposure (the first *arrow* in Fig. 1; 6 Gy/min). The source is withdrawn to terminate the exposure. Depending on the cell preparation, between 30 and 40% of A431 cells (195 total cells measured in 11 different experiments) responded to a 3-Gy (30 s) radiation exposure and produced an increase in ROS/RNS as indicated by an increase in DCF fluorescence (Fig. 1). For most responding cells, the increase in ROS/RNS commences during the radiation exposure and continues for approximately 2–5 min after irradiation before returning to basal levels. Two of the responding cells demonstrate a sustained rise in DCF fluorescence that persisted for at least 15 min after irradiation. The remaining cells show no change in DCF fluorescence in response to radiation (although they do so to hydrogen peroxide) in

the time period examined. Similar experiments were performed with MCF-7 and MDA-MB-231 breast carcinoma cells, PC-3 and DU-145 prostate carcinoma cells, CHO cells, and osteosarcoma 143BTK$^-$ ρ^+ cells. In all of the cases, similar responses were seen including the immediate and transient increase in ROS/RNS in 30–50% of the cells after a radiation exposure of 3–4 Gy.

The Number of Cells with a Transient Enhancement in ROS/RNS Generation Increases with Radiation Dose. In Fig. 2*A*, the percentage of cells that produce ROS/RNS is plotted *versus* radiation dose (upper curve). The average fluorescence intensity change/cell (designated Δ in Fig. 1) is graphed as a function of radiation dose in the lower curve. There is a progressive increase in the number of cells that respond to increasing radiation dose with a burst of ROS/RNS generation. However, there was no apparent relationship between radiation dose and Δ, the average fluorescence intensity change/cell. For the cell preparation used in Fig. 2, Δ varied by 30% among responding cells regardless of the radiation dose between 1 and 10 Gy. Similar results were obtained with two other cell preparations. These data suggest that the cellular response in terms of amount of ROS/RNS generated is all-or-nothing in this radiation dose range. In the cell preparations used to evaluate the dose response, no cells exhibited a sustained increase in ROS/RNS after radiation.

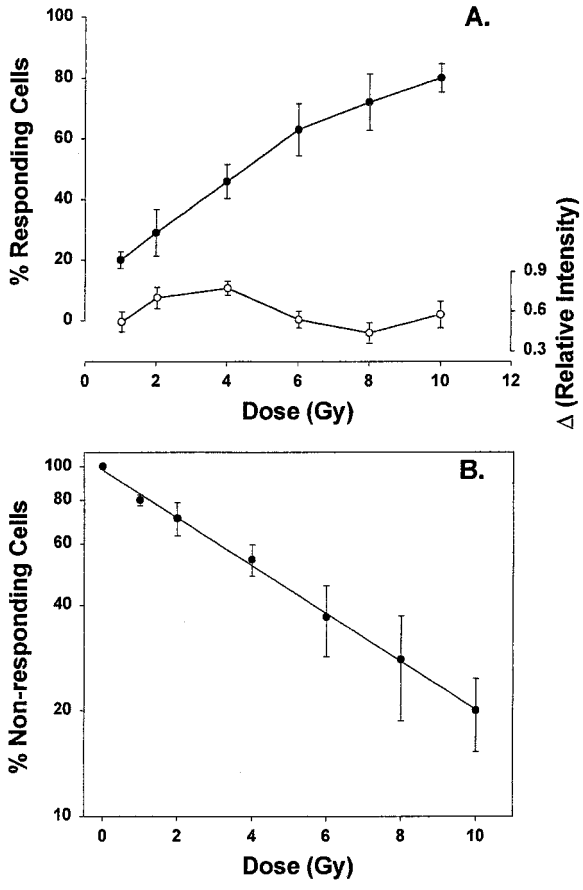

Fig. 2. Dose response analysis of radiation-induced ROS/RNS generation in A431 cells. *A*, *top curve* (*left hand axis*), number of cells with enhanced DCF fluorescence after irradiation as a function of dose. This graph is the average of two separate experiments with a total number of 80 cells for each radiation dose; *bars*, ± SE. *Bottom curve* (*right hand axis*), Δ as defined in Fig. 1 is plotted as a function of radiation dose. Because the DCF fluorescence signal cannot be calibrated in terms of absolute amount of ROS/RNS, relative changes were quantified as the fluorescence intensity difference before and after the transient rise in DCF fluorescence (Δ in Fig. 1). Twenty cells from one cell preparation were irradiated at each dose, and the data points are the average Δ ± SE for the responding cells. *B*, a semilog plot of the data in *A* (*upper curve*) graphed in terms of the nonresponding fraction of cells as a function of radiation dose. The linear regression analysis was performed by SigmaPlot software.

A more traditional radiobiological semilog plot of the fraction of nonresponding cells *versus* radiation dose can also be used to examine the data. Results from the upper curve of Fig. 2*A* are graphed in this manner and shown in Fig. 2*B*. A linear regression analysis of the semilog plot ($r^2 > 0.99$) reveals a logarithmic relationship between the number of nonresponding cells and radiation dose. According to classical target theory, this result is consistent with a single target type.

Radiation-induced ROS/RNS Are Mitochondrial in Origin. Electron leakage from mitochondrial electron transport is the primary source of ROS generation in nonphagocytic cells. To provide evidence that the radiation-induced increases in ROS/RNS were dependent on mitochondrial electron transport, we measured radiation-stimulated ROS/RNS production in cells that are deficient in mitochondrial electron transport. Osteosarcoma 143TK$^-$ ρ^o cells completely lack mitochondrial DNA and are incapable of electron transport/oxidative phosphorylation (22, 30). Fig. 3 shows representative DCF fluorescence tracings of osteosarcoma 143TK$^-$ ρ^o and the parental ρ^+ cells. None of the ρ^o cells examined exhibit a radiation-stimulated increase in ROS/RNS generation ($n = 65$; four cell preparations). Furthermore, the basal rate of ROS/RNS production by ρ^o cells before irradiation is considerably lower compared with that of ρ^+ cells, as would be expected for cells with mitochondria incapable of electron transport (31). Consistent with the other respiratory competent cell lines examined, approximately 50% of the parental ρ^+ cells respond to 4-Gy radiation with a transient increase in ROS/RNS generation ($n = 90$; five cell preparations). We conclude that mitochondrial respiration is necessary for the radiation-induced ROS/RNS production.

Studies with rotenone, an electron transport complex I poison, provided additional evidence for the involvement of mitochondrial electron transport in radiation-induced ROS/RNS production. Incubating cells with 10 μM rotenone stimulated ROS/RNS generation because blocking electron transport through complex I siphons electrons directly to O_2 at complex I, resulting in the partial reduction of O_2 and ROS generation. No further enhancement of ROS/RNS generation was observed after radiation exposure (data not shown).

Other potential cellular sources of ROS were examined. Inhibitors of phospholipase A2 (50 μM PX52 for 30 min; Ref. 32) and P450 cytochrome oxidase (100 μM proadifen for 30 min; Ref.33) are ineffective in blocking radiation-induced ROS/RNS in A431 cells ($n = 40$ cells; two independent experiments for each inhibitor; data not shown). Hence, these nonmitochondrial ROS/RNS sources are not involved in the radiation-induced ROS/RNS generation.

Radiation Stimulates a Reversible Mitochondrial Permeability Transition. The above studies point to the mitochondria as the source of radiation-induced ROS/RNS production. Previous studies (34) have demonstrated that induction of the mitochondrial permeability transition can stimulate ROS/RNS generation. CsA is an effective inhibitor of the permeability transition, and thus we have used this reagent to test for the possible relationship of the permeability transition and radiation-induced ROS/RNS generation (25–28, 31, 35). Preincubating A431 cells for 30 min with 1 μM CsA completely inhibited radiation-induced ROS/RNS generation in all of the cells examined ($n = 70$ cells; four separate experiments at 4 Gy). CsH, a CsA analogue that is ineffective at blocking the mitochondrial permeability transition (25), did not inhibit radiation-induced ROS/RNS generation (13 of 30 cells responded to 4 Gy, compared with 16 of 34 control irradiated cells; two experiments). These results are consistent with a potential role for the mitochondrial permeability transition in the radiation-induced ROS/RNS formation.

Propagation of the mitochondrial permeability transition from one mitochondrion to another in cells and *in vitro* is Ca^{2+}-dependent,

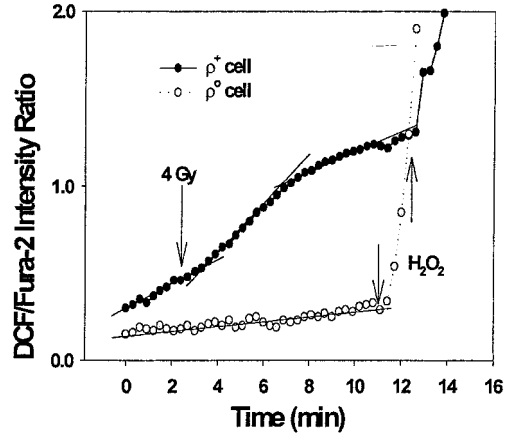

Fig. 3. Mitochondrial electron transport is necessary for radiation-induced ROS/RNS. DCF fluorescence measurements are as described in the text and legend to Fig. 1. The radiation dose was 4 Gy. Dye-loading conditions and fluorescence measurements are as described for A431 cells for both the parental ρ^+ and electron transport-deficient ρ^o osteosarcoma cells.

involving localized changes in cytosolic [Ca^{2+}] and the uptake and release of mitochondrial Ca^{2+} (20, 35, 36). If radiation-induced ROS/RNS generation requires the mitochondrial permeability transition and its propagation, then inhibiting the Ca^{2+}-dependent propagation should also block radiation-induced ROS/RNS production. We tested the effects of attenuating changes in cytosolic [Ca^{2+}] by overexpression of the Ca^{2+}-binding protein, calbindin 28K, and by equilibrating cells with the intracellular Ca^{2+} chelator, BAPT/AM (23). For the experiments with calbindin 28K, CHO cells are used because of the much higher transfection efficiency of these cells (>80%, determined with a plasmid encoding a green fluorescent protein) compared with A431 cells (<10%). At a radiation dose of 4 Gy, approximately 50% of the CHO cells transfected with the empty vector (28 of 60 cells; $n = 3$ experiments) exhibit significant radiation-induced ROS/RNS. A similar result is also obtained with nontransfected CHO cells. In contrast, radiation-stimulated ROS/RNS is observed in less than 10% of the calbindin 28K-expressing cells (5 of 58; $n = 3$ experiments). This Ca^{2+} dependency is confirmed in experiments where A431 cells are equilibrated with the membrane permeant acetooxymethyl ester derivative of BAPT/AM (10 μM for 60 min during equilibration with dihydro-DCF). This treatment completely blocks radiation-induced ROS/RNS production (40 cells; $n = 2$ experiments).

Induction of a mitochondrial permeability transition with intact cells was initially assessed by measurement of CsA-sensitive changes in mitochondrial $\Delta\Psi$ with the fluorescent dye, TMRE (20, 25, 36). This dye is cationic and concentrates in mitochondria because of the high negative inside $\Delta\Psi$. Under the loading conditions used, the high dye concentration within polarized mitochondria results in self-quenching, and upon depolarization, redistribution of the dye into the cytoplasm results in enhanced fluorescence (20). Fig. 4 shows the average fluorescence measurements of four responding cells in comparison with the average response of six nonresponding cells on a single coverslip with a radiation exposure of 4 Gy. Before irradiation, there is a gradual decrease in fluorescence attributable in part to photobleaching. Upon irradiation, there is a 3–5-min transient increase in fluorescence, indicative of depolarization, followed by a decrease in TMRE fluorescence, indicative of repolarization. As expected, addition of the protonophore, FCCP, results in an increase in fluorescence (depolarization). The transient depolarizing effect of radiation on mitochondrial $\Delta\Psi$ is consistently observed in about 50% of the cells at this dose of radiation (37 of 80 cells; four experiments). The nonresponding cells demonstrate no change in fluorescence after irradiation other than the baseline decrease attributable to photobleaching. Pretreating cells for 30 min with 1 μM CsA completely abrogated the radiation-induced depolarization in all of the cells examined.

We also compared the mitochondrial $\Delta\Psi$ responses of osteosarcoma ρ^+ and ρ^o cells with radiation. The parental ρ^+ cells behave identically to A431 cells in their response to radiation exposure, whereas the ρ^o cells show no change in TMRE fluorescence upon irradiation (data not shown). The FCCP-stimulated enhancement of TMRE fluorescence (a relative measure of mitochondrial $\Delta\Psi$) for ρ^o cells is 30% that observed for wild-type ρ^+ cells. Thus, osteosarcoma ρ^o mitochondria are less polarized relative to wild type, a finding demonstrated by other investigators (37). Nonetheless, the $\Delta\Psi$ data are consistent with the DCF measurements and a requirement for mitochondrial electron transport in the cellular response to radiation.

Changes in fluorescence of mitochondrial entrapped calcein were also used as a measure of the permeability transition (25, 26, 28). Activation of the permeability transition enhances the permeability of mitochondria to molecules of M_r 1600 or less (35). Previous investigators have monitored this enhanced permeability by loading cells with acetooxymethylester of the fluorescent dye, calcein, and relying on cytoplasmic and mitochondrial esterases to cleave the ester entrapping the charged dye. Mitochondrial calcein is visualized by simultaneously quenching cytosolic calcein fluorescence with $CoCl_2$. Mitochondria do not actively transport Co^{2+} nor are their respiratory properties significantly impaired by Co^{2+} (25, 26, 28). As a positive control, cells are treated with either ionomycin or thapsigargin (an inhibitor of the endoplasmic reticulum Ca^{2+} pump) that raise cytosolic [Ca^{2+}] and, by so doing, trigger the mitochondrial permeability transition. With Co^{2+} present, the calcein fluorescence is seen in the perinuclear region typical of mitochondrial staining with mitochondrial specific dyes (Fig. 5 inset and Refs. 25–28, 38).

Fig. 5 shows the results of an experiment where a radiation-induced mitochondrial pore opening is detected by the loss of mitochondrial calcein fluorescence. The data shown are for cells from one coverslip of A431 cells, representative of two independent experiments. For clarity, cells responding to radiation with changes in calcein fluorescence are shown in Fig. 5*A* in comparison with the nonresponding cells in Fig. 5*B*. Irradiation at 4 Gy elicits a transient decrease in mitochondrial calcein fluorescence in approximately 50% of the cells. In two independent experiments, 34 of 75 cells responded with a

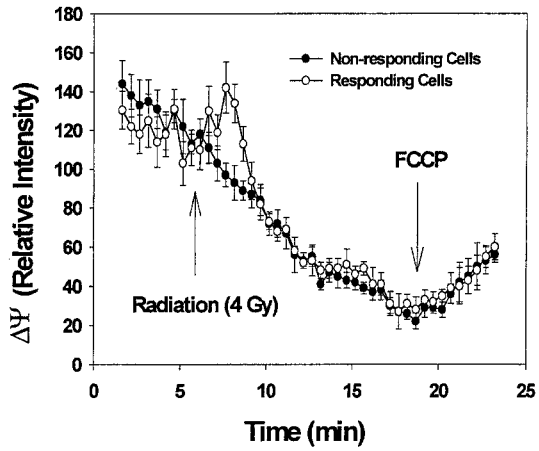

Fig. 4. Radiation induces a mitochondrial permeability transition as measured by changes in mitochondrial $\Delta\Psi$. The results show the average fluorescence readings (± SE) of four responding and six nonresponding A431 cells on a single coverslip and irradiated where indicated at 4 Gy. FCCP was added to a final concentration of 1 μM. For clarity, only every other data point is shown.

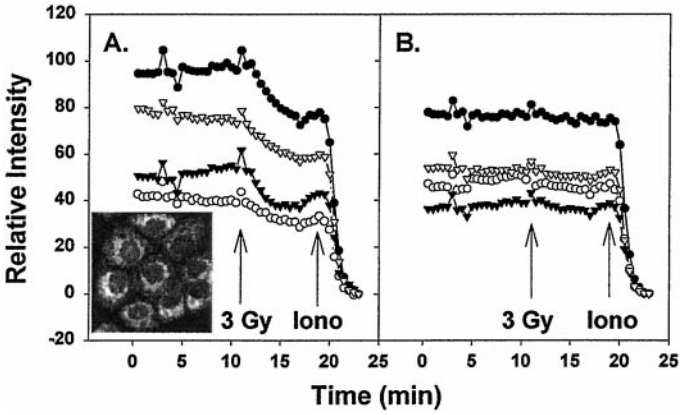

Fig. 5. Mitochondrial permeability transition monitored by calcein fluorescence. Cells were loaded with calcein and Co^{2+} as described in the text. The fluorescence image shows a group of cells excited at 490 nm, the excitation wavelength maximum for calcein. Emission was monitored at 530 nm. Results shown are for cells from a single coverslip divided into cells that responded to a 4-Gy radiation exposure with a decrease in calcein fluorescence of >10% (*A*) or <10% (*B*).

decrease in calcein fluorescence of at least 15% of the initial intensity with an average decrease of 23 ± 7% (Fig. 5*A*). Subsequent incubation with ionomycin (or thapsigargin; data not shown) to trigger a sustained permeability transition stimulates the complete loss of calcein fluorescence in all of the 75 cells. The radiation-, ionomycin-, and thapsigargin-induced decreases in mitochondrial calcein fluorescence are not observed in cells incubated for 30 min with 1 μM CsA (two independent experiments; 65 cells). These results corroborate the data obtained with TMRE, demonstrating that CsA-sensitive mitochondrial pore formation can be induced by radiation. These effects also correlate temporally with the radiation-induced $\Delta\Psi$ depolarization and ROS/RNS generation.

Measurement of ROS/RNS in Bulk Assays. A microtiter plate assay for measuring ROS/RNS generation was developed to verify that our measurements of radiation-induced ROS/RNS are independent of the radiation source and microscopic detection system. A ^{60}Co source is used in these experiments, but because of the physical separation between the radiation device and microplate reader, the earliest time point measured is 10 min after irradiation.

Fig. 6*A* shows the results from three separate experiments measuring DCF fluorescence. Irradiation is carried out in a 96-well plate, and the nonirradiated samples are shielded with a lead brick. The *filled bars* representing the nonirradiated samples indicate variability in the dye loading from one cell preparation to another, in agreement with the microscopic analysis. Nonetheless, a comparison of the nonirradiated samples with the irradiated cells (*open bars*) demonstrates that radiation significantly increases ROS/RNS generation above that because of endogenous metabolism (10–25%; Student's *t* test; $P < 0.001$). The microtiter plate assay was used to test possible inhibitors of mitochondrial function on radiation-induced ROS/RNS generation. In Fig. 6*B*, CsA and CsH, the inactive CsA analogue, are compared in terms of their relative effects on the amount of DCF fluorescence generated between irradiated and nonirradiated cells. The effect of BA, a specific inhibitor of the mitochondrial adenine nucleotide translocator, that blocks the permeability transition was also examined (39). CsH (1–10 μM) has no significant effect on the amount of ROS/RNS generated by radiation. In contrast, the amount of ROS/RNS stimulated by radiation progressively decreases as the concentration of CsA increases over the same concentration range. BA at 50 μM is only partially effective at inhibiting radiation-induced ROS/RNS. The incomplete inhibition of radiation-induced ROS/RNS by CsA (or BA) in the microtiter assay contrasts with the apparent complete inhibition observed in the microscopic analysis. The most probable reason for this apparent discrepancy is dye leakage from the cells, which occurs in both assays but is detectable only in the microtiter plate assay. In the microscopic analysis, there is a continuous recording and subtraction of background fluorescence. This is in contrast to the microtiter assay where there is a continuous build-up of extracellular DCF, which is insensitive to CsA or BA.

Radiation-stimulated MAP Kinase Activity Requires Activation of the Mitochondrial Permeability Transition. Previous studies from this and other laboratories (9, 12, 29, 40) have demonstrated that ionizing radiation activates MAP kinase. The underlying mechanism of activation is unclear but appears to involve ROS (9, 41) and Ca^{2+}. Blocking radiation-stimulated cytoplasmic Ca^{2+} transients with an intracellular Ca^{2+} chelator inhibits MAP kinase activation (29). These requirements for activation and the results described above prompted us to test whether inhibitors of the mitochondrial permeability transition, BA and CsA, also inhibit radiation-induced MAP kinase activation. We also compared ρ^o and ρ^+ cells.

As described previously (29) for A431 cells, low doses of radiation stimulate a transient 3–4-fold activation of MAP kinase activity that is maximal at about 4 min after irradiation (Fig. 7*A*). Pretreating A431 cells for 10 min with 50 μM BA had no significant effect on basal MAP kinase activities but completely inhibited the radiation-induced MAP kinase activation. Identical results were obtained in CHO cells with BA and CsA completely inhibiting radiation-induced MAP kinase activation (data not shown). These results are consistent with a

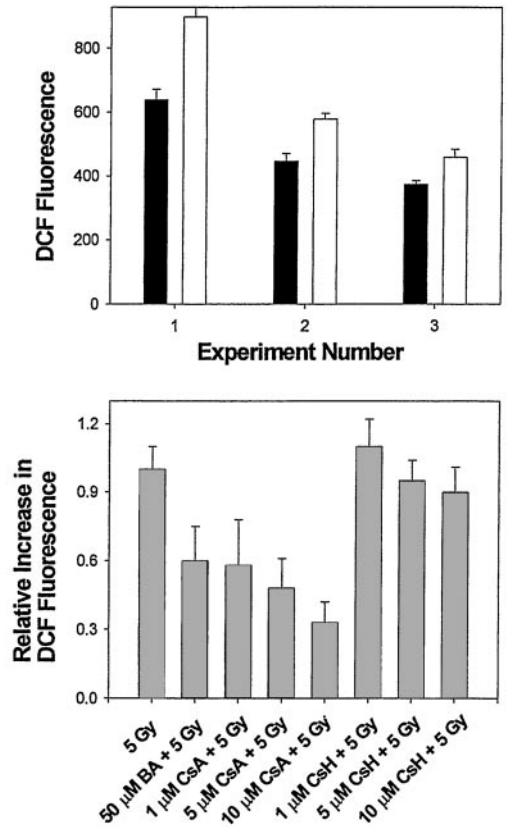

Fig. 6. Measurement of ROS/RNS by a microtiter plate assay. *A*, results are shown for three cell preparations with radiation-induced ROS/RNS measured with DCF fluorescence as described in the text. Each data point represents the average of readings from eight wells ± SE. Student's *t* test calculates $P < 0.001$ for the difference between control and irradiated samples in the three experiments. *B*, cells were incubated at the given concentrations of CsA, CsH, or 50 μM BA for 30 min before radiation exposure. The difference in DCF fluorescence of irradiated and nonirradiated samples (eight wells each ± SE) was calculated for each drug concentration and plotted as a percentage of the nondrug-treated control.

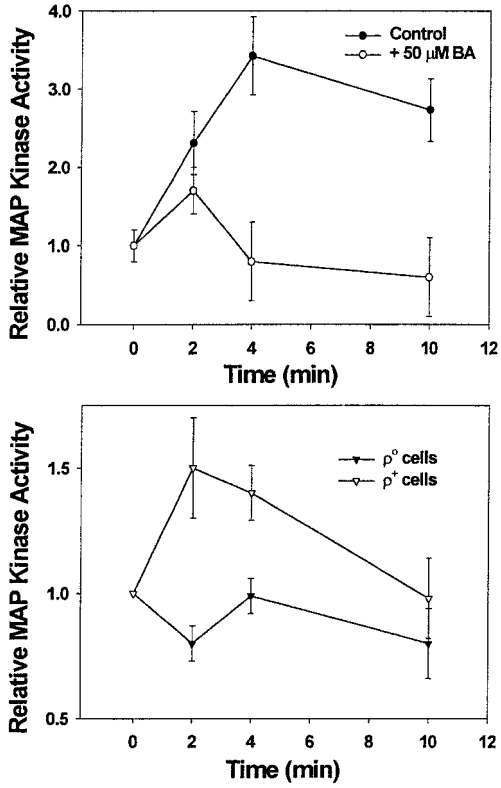

Fig. 7. Radiation-induced MAP kinase activation is dependent on the mitochondrial permeability transition. MAP kinase activity was measured as described in "Materials and Methods" and calculated in terms of activity relative to time = 0 nonirradiated control. The radiation dose in both sets of experiments was 2 Gy, and time points are referenced to the end of the radiation period (t = 0 min). *Top*, average results (± SE) from three separate experiments with A431 cells with (○) and without (●) treatment with 50 μM BA for 10 min prior radiation exposure. *Bottom*, the average results (± SE) from three separate experiments with ρ^o (▼) and ρ^+ (▽) cells.

radiation-induced mitochondrial permeability transition being necessary for MAP kinase activation. This conclusion was further supported by studies comparing the ρ^o and ρ^+ osteosarcoma cells. Basal MAP kinase activities of these two cells were approximately identical. The radiation-induced MAP kinase response for ρ^+ cells, although not as robust as observed for A431 cells, was consistently observed with all of the three cell preparations examined (Fig. 7*B*). In contrast, radiation was ineffective in stimulating MAP kinase in the mitochondrial electron transport-deficient ρ^o cells. These findings combined with the pharmacological experiments strongly indicate that activation of the MAP kinase signal transduction pathway by radiation requires a radiation-inducible and reversible mitochondrial permeability transition.

DISCUSSION

The present investigation has demonstrated that ionizing radiation in the therapeutic dose range stimulates a transient cellular generation of ROS/RNS. Temporally coincident is a radiation-induced reversible depolarization of the mitochondrial $\Delta\Psi$ and decrease in mitochondrial entrapped calcein fluorescence, both hallmarks of the mitochondrial permeability transition. The amount of ROS/RNS generated is relatively constant over the dose range tested, but the number of cells that respond increases with the dose. The radiation-induced ROS/RNS generation, $\Delta\Psi$ depolarization, and calcein release are inhibited by CsA but not by the structural analogue, CsH. Overexpression of the Ca^{2+}-binding protein calbindin 28K or treatment of cells with BAPTA/AM, an intracellular Ca^{2+} chelator, also effectively block radiation-induced ROS/RNS. The increased ROS/RNS generation observed with radiation is common to all of the cell types examined but for one important exception, the mitochondrial DNA-less ρ^o osteosarcoma cells. In contrast to the wild-type parental cell line, ρ^o cells lack a complete electron transport chain and demonstrate neither radiation-induced ROS/RNS nor $\Delta\Psi$ depolarization.

Given the number of ionization events/cell at the radiation doses used herein (2000 Gy; 5), it is unlikely that significant numbers of mitochondria undergo the permeability transition as a direct consequence of a primary ionization event. However, the spatiotemporal interactions of mitochondria within cells suggest the following model of propagative signaling for radiation-enhanced cellular ROS/RNS generation. In this model, ionizing radiation initiates an oxidative event within a mitochondrion that results in the localized release of Ca^{2+}. Adjacent mitochondria take up the Ca^{2+} and, as a consequence, undergo the mitochondrial permeability transition (exemplified by $\Delta\Psi$ depolarization) and release Ca^{2+} to further propagate the signal to adjacent mitochondria. Elevated mitochondrial Ca^{2+} levels and/or $\Delta\Psi$ depolarization can enhance mitochondrial ROS/RNS generation (34), although this may not be the only source of elevated ROS/RNS, as discussed below.

For such a mechanism to be viable requires that mitochondria are in close proximity to each other within a cell and that the permeability transition is reversible. Recent studies (20, 42–44) indicate that these requirements are fulfilled. In dividing cells, a substantial fraction of the cellular mitochondria are recruited to and concentrated near the nucleus as part of the mitochondrial replication component of cell division (38). This is readily apparent in the inset to Fig. 5. Three-dimensional optical microscopic analysis has further revealed that mitochondria form a large constantly changing but interconnected tubular network (42). Functional studies (42–44) have demonstrated subcellular heterogeneity of mitochondrial energization in intact cells but also cell-wide coordinated redox transitions and metabolic waves within cells that necessitate close mitochondrial proximity. Moreover, isolated mitochondria can be induced to propagate a reversible permeability transition (20). In these latter studies, the addition of Ca^{2+} to immobilized mitochondria at one corner of a coverslip was shown by confocal microscopy to initiate a wave of mitochondrial depolarization/repolarization in synchrony with Ca^{2+} uptake/release that spreads across the coverslip.

Previous investigations (17, 25–27, 31) have primarily focused on the irreversible mitochondrial permeability transition that is associated with cells undergoing apoptosis. However, electrophysiological studies (35, 36, 45) of the permeability transition pore have demonstrated multiple conductance states, one of which corresponds to a half-conductance state of 500 pico seconds compared with the fully open conformation of 1200 pS. The former may correspond to the low conductance state associated with a reversible switching between permeable and impermeable states or "flickering" that has been observed by a number of investigators (reviewed in Refs. 35, 36, 45). Although we have no direct evidence as yet, we suspect that the mitochondrial permeability transition observed here as the radiation-induced transient $\Delta\Psi$ depolarization and mitochondrial calcein fluorescence decrease corresponds to a low conductance permeability pore.

A previous study (31) with U937 ρ^o cells demonstrated that tumor necrosis factor stimulated a mitochondrial permeability transition as evidenced by enhanced ROS generation and mitochondrial $\Delta\Psi$ depolarization. This fits with the knowledge that electron transport-deficient ρ^o cells differ from their normal ρ^+ counterparts only in RNA components required for mitochondrial protein synthesis and some structural proteins of the electron transport chain encoded by mitochondrial DNA (30). Other mitochondrial functions encoded by nuclear DNA (*e.g.*, adenine nucleotide translocator, a presumed compo-

nent of the permeability channel) appear to be intact (31, 37). The finding of tumor necrosis factor-induced mitochondrial permeability transition in U937 ρ^o cells would appear to be in conflict with the present study showing an absence of a radiation-induced permeability transition in osteosarcoma ρ^o cells. However, the results from these studies are distinguishable by two important features. Firstly, the present study demonstrates a reversible permeability transition in the parental ρ^+ cells (transient $\Delta\Psi$ depolarization and ROS/RNS generation) in contrast to the irreversible sustained effects on these two parameters observed with tumor necrosis factor treatment. Secondly, the radiation-induced permeability transition is observed during the radiation exposure and within the first few min after irradiation. The irreversible transition, on the other hand, is detected hours after treatment and is associated with apoptosis. Thus, these two studies, although measuring similar parameters, are observing either fundamentally different states of the channel (*e.g.*, different conductance states) or different functional consequences of its activation.

Numerous studies on the effects of ionizing radiation on mitochondrial structure and function have been reported during the past 40 years. Most have focused on events hours after irradiation (Refs. 46, 47, and references therein). Where the effects of ionizing radiation have been examined with isolated mitochondria, no observable changes in respiration or other indices of mitochondrial function have been observed except at very high doses of radiation. In these studies, relatively dilute solutions of mitochondria are used, and the mitochondria are prepared and incubated in the absence of Ca^{2+}. Thus, the effects of relatively low doses of radiation on the propagation of the mitochondrial permeability transition would not be observed. Investigations currently underway in this laboratory are testing whether low doses of radiation can stimulate the permeability transition with isolated mitochondria preloaded with Ca^{2+}.

The dose response analysis is consistent with the proposed propagation mechanism. Dose escalation results in an increasing number of responding cells but with a relatively constant amount of ROS/RNS generated/cell. This suggests that a threshold in the number of mitochondria activated initially would need to be surpassed. Once the threshold is surpassed, a relatively constant number of mitochondria defined by their spatial concentration within a cell would subsequently undergo the permeability transition and produce ROS/RNS. The logarithmic relationship between the fraction of nonresponding cells and the radiation dose (Fig. 2*B*) is consistent with a single radiation target.

The dose response obtained by single cell analysis also has important implications for studies on signal transduction pathways activated as a consequence of cytoplasmic irradiation. The simplest interpretation of a dose response based on the analysis of a population of cells is that with increasing dose there is an increase in activity on a per cell basis. Our results with single cell analysis, on the other hand, would suggest that the magnitude of activation is relatively independent of dose, but with increasing dose there are increased numbers of cells with an activated signal transduction pathway. For A431 cells irradiated within the therapeutic dose range (1–2 Gy), this means that the signal transduction pathways dependent on cytoplasmic-generated ROS/RNS (*e.g.*, growth factor receptors, stress kinases, and transcription factors such as nuclear factor κB; Refs. 1, 7, 9, 41, 48) would be activated in only 20–30% of the cells. However, the degree of activation in these responding cells is much greater than indicated from the average obtained in bulk assays of responding and nonresponding cells. Future studies relating specific signal transduction pathways activated by ROS/RNS with downstream cellular consequences may need to address this response heterogeneity.

Oxidation of dihydro-DCF was used to detect ROS/RNS. This dye is well characterized in its response to ROS/RNS, but its fluorescence response does not discriminate between hydroxyl radical, peroxynitrite, or ROS generated from hydrogen peroxide in the presence of a peroxidase (16, 24). Our evidence demonstrates a role for the mitochondrion in amplifying/transmitting a signal that results in ROS/RNS production but does not indicate that mitochondria necessarily generate the cellular ROS/RNS after a radiation exposure. The inhibitor results would appear to eliminate ROS derived from phospholipase A2 and P450 enzymes. Ongoing studies are seeking to identify the ROS/RNS involved. This effort may provide evidence for source(s) other than mitochondria, *e.g.*, the plasma membrane NADPH oxidase (49) and constitutive nitric oxide synthases (50), that are activated by mechanisms involving the mitochondrial permeability transition.

In summary, our results demonstrate that cytoplasmic primary ionization events after exposure of cells to clinically relevant doses of ionizing radiation are amplified by a mechanism involving a mitochondrial permeability transition and further production of ROS/RNS. This amplification mechanism appears necessary for radiation-induced activation of downstream signal transduction pathways such as MAP kinase. We speculate that the significance of these findings is not limited to clinical levels of radiation, but that similar processes provide a general mechanism by which cells sense and respond to oxidative events within the cytoplasm.

REFERENCES

1. Schmidt-Ullrich, R. K., Dent, P., Grant, S., Mikkelsen, R. B., and Valerie, K. Signal transduction and cellular radiation responses. Radiat. Res., *153:* 245–257, 2000.
2. Elledge, S. J. Cell cycle checkpoints: preventing an identity crisis. Science (Wash. DC), *274:* 1664–1672, 1996.
3. Brown, A. L., Lee, C. H., Schwarz, J. K., Mitiku, N., Piwnica-Worms, H., and Chung, J. H. A human Cds1-related kinase that functions downstream of ATM protein in the cellular response to DNA damage. Proc. Natl. Acad. Sci. USA, *96:* 3745–3750, 1999.
4. Chen, P., Gatei, M., O'Connell, M. J., Khanna, K., Bugg, S. J., Hogg, A., Scott, S. P., Hobson, K., and Lavin, M. F. Chk1 complements the G_2/M checkpoint defect and radiosensitivity of ataxia-telangiectasia cells. Oncogene, *18:* 249–256, 1999.
5. Ward, J. DNA damage as the cause of ionizing radiation-induced gene activation. Radiat. Res., *138* (Suppl.)*:* 85s–88s, 1994.
6. Todd, D., and Mikkelsen, R. B. Ionizing radiation induces a transient increase in cytosolic free [Ca^{2+}] in human epithelial tumor cells. Cancer Res., *54:* 5234–5230, 1994.
7. Schmidt-Ullrich, R. K., Mikkelsen, R. B., Dent, P., Todd, D., Valerie, K., Kavanagh, B., Contessa, J., Rorrer, K., and Chen, P. Radiation-induced proliferation of the human A431 squamous carcinoma cells is dependent on EGFR tyrosine phosphorylation. Oncogene, *15:* 1191–1197, 1997.
8. Haimovitz-Friedman, A., Kan, C-C., Ehleiter, D., Persaud, R., McLaughlin, M., Fuks, Z., and Kolesnick, R. Ionizing radiation acts on membranes to generate ceramide and initiate apoptosis. J. Exp. Med., *180:* 525–535, 1994.
9. Stephenson, M. A., Pollock, S., Coleman, C., and Calderwood, S. X-irradiation, phorbol esters, and H_2O_2 stimulate mitogen-activated protein kinase activity in NIH-3T3 cells through the formation of reactive oxygen intermediates. Cancer Res., *54:* 12–15, 1994.
10. Reardon, D. B., Contessa, J. N., Mikkelsen, R. B., Valerie, K., Amir, C., Dent, P., and Schmidt-Ullrich, R. K. Dominant negative EGFR-CD533 and inhibition of MAPK modify JNK1 activation and enhance radiation toxicity of human mammary carcinoma cells. Oncogene, *18:* 4756–4766, 1999.
11. Kasid, U., Suy, S., Dent, P., Ray, S., Whiteside, T. L., and Sturgill, T. W. Activation of Raf by ionizing radiation. Nature (Lond.), *382:* 813–816, 1996.
12. Kharbanda, S., Saleem, A., Shafman, T., Emoto, Y., Weichselbaum, R., and Kufe, D. Activation of the pp90rsk and mitogen-activated serine/threonine protein kinases by ionizing radiation. Proc. Natl. Acad. Sci. USA, *91:* 5416–5420, 1994.
13. Roots, R., and Okada, S. Protection of DNA molecules of cultured mammalian cells from radiation induced single strand scissions by various alcohols and SH compounds. Int. J. Radiat. Biol., *21:* 329–342, 1972.
14. Narayanan, P., Goodwin, E., and Lehnert, B. α particles initiate biological production of superoxide anions and hydrogen peroxide. Cancer Res., *57:* 3963–3971, 1997.
15. Morales, A., Miranda, M., Sanchez-Reyes, A., Biete, A., and Fernandez-Checa, J. Oxidative damage of mitochondrial and nuclear DNA induced by IR in human hepatoblastoma cells. Int. J. Radiat. Oncol. Biol. Phys., *42:* 191–204, 1998.
16. Crow, J. P. Dichlorodihydrofluorescein and dihydrorhodamine 123 are sensitive indicators of peroxynitrite *in vitro*: implications for intracellular measurement of reactive nitrogen and oxygen species. Nitric Oxide, *1:* 145–157, 1997.
17. Backway, K. L., McCulloch, E. A., Chow, S., and Hedley, D. W. Relationships between the mitochondrial permeability transition and oxidative stress during ara-C toxicity. Cancer Res., *57:* 2446–2451, 1997.
18. Costantini, P., Chernyak, B. V., Petronelli, V., and Bernardi, P. Modulation of the mitochondrial permeability transition pore by pyridine nucleotides and dithiol oxidation at two separate sites. J. Biol. Chem., *271:* 6746–6751, 1996.

19. Skulachev, V. Why are mitochondria involved in apoptosis? FEBS Lett., *397:* 7–10, 1996.
20. Ichas, F., Jouavile, L. S., and Mazat, J. P. Mitochondria are excitable organelles capable of generating and conveying electrical and calcium signals. Cell, *89:* 1145–1153, 1997.
21. Halestrap, A., Woodfield, K., and Connern, C. Oxidative stress, thiol reagents, and membrane potential modulate the MPT by affecting nucleotide binding to the nucleotide translocator. J. Biol. Chem., *272:* 3346–3354, 1997.
22. King, M. P., and Attardi, G. Isolation of human cell lines lacking mitochondrial DNA. Methods Enzymol., *264:* 304–313, 1996.
23. Guo, Q., Christakos, S., Robinson, N., and Mattson, M. P. Calbindin D28k blocks the proapoptotic actions of mutant presenilin 1: reduced oxidative stress and preserved mitochondrial function. Proc. Natl. Acad. Sci. USA, *95:* 3227–3232, 1998.
24. Possel, H., Noack, H., Augustin, W., Keilhoff, G., and Wolf, G. 2,7-dihydrodichlorfluoroscein diacetate as a fluorescent marker for peroxynitrite formation. FEBS Lett., *416:* 175–178, 1997.
25. Petronelli, V., Miotto, G., Canton, M., Brini, M., Colonna, R., Bernardi, P., and Di Lisa, F. Transient and long-lasting openings of the mitochondrial permeability transition pore can be monitored directly in intact cells by changes in mitochondrial calcein fluorescence. Biophys. J., *76:* 725–734, 1999.
26. Minamikawa, T., Williams, D., Bowser, D., and Nagley, P. Mitochondrial permeability transition and swelling can occur reversibly without inducing cell death in intact human cells. Exp. Cell Res., *246:* 26–37, 1999.
27. Lemasters, J., Nieminen, A., Qian, T., Trost, L., Elmore, S., Nishimura, Y., Crowe, R., Cascio, W., Bradham, C., Brenner, D., and Herman, B. The mitochondrial permeability transition in cell death: a common mechanism in necrosis, apoptosis, and autophagy. Biochim. Biophys. Acta, *1366:* 177–196, 1998.
28. Scorrano, L., Petronelli, V., and Bernardi, P. On the voltage dependence of the mitochondrial permeability transition pore. J. Biol. Chem., *272:* 12295–12299, 1997.
29. Kavanagh, B., Dent, P., Schmidt-Ullrich, R. K., Chen, P., and Mikkelsen, R. B. Calcium-dependent stimulation of mitogen-activated protein kinase activity in A431 cells by low doses of ionizing radiation. Radiat. Res., *149:* 579–587, 1998.
30. Gray, M. W. Origin and evolution of mitochondrial DNA. Annu. Rev. Biochem., *5:* 25–50, 1989.
31. Marchetti, P., Susin, S. A., Decausin, D., Gamen, S., Castedo, M., Hirsch, T., Zamami, N., Naval, J., Senik, A., and Kroemer, G. Apoptosis-associated derangement of mitochondrial function in cells lacking DNA. Cancer Res., *56:* 2033–2038, 1996.
32. Dorsam, G. Group IIA phospholipase A2s elevated in uremic syndrome and diphenyleneiodium chloride blocks cytokine-induced upregulation of group IIA phospholipase A2 in rat mesangial cells (Thesis). Richmond, VA: Medical College of Virginia, Richmond, 1998.
33. Salvemini, D., Pistelli, A., and Vane, O. Vascular and antiplatelet actions of 1,2- and 1,3-glyceryl dinitrate. Br. J. Pharmacol., *108:* 162–169, 1993.
34. Vercesi, A. E., Kowaltowski, A. J., Grijalba, M. T., Meinicke, A. R., and Castilho, R. F. The role of reactive oxygen species in mitochondrial permeability transition. Biosci. Rep., *17:* 43–52, 1997.
35. Zoratti, M., and Szabo, I. The mitochondrial permeability transition. Biochem. Biophys. Acta, *1241:* 139–176, 1995.
36. Ichas, F., and Mazat, J. P. From calcium signaling to cell death: two conformations for the MPT pore. Switching from low- to high-conductance state. Biochim. Biophys. Acta, *1366:* 33–50, 1998.
37. Buchet, K., and Godinot, C. Functional F1-ATPase essential in maintaining growth and membrane potential of human mitochondrial DNA-depleted r^o cells. J. Biol. Chem., *273:* 22983–22989, 1998.
38. Davis, A., and Clayton, D. *In situ* localization of mitochondrial DNA replication in intact mammalian cells. J. Cell Biol., *135:* 883–893, 1996.
39. Zamzami, N., Susin, S. A., Marchetti, P., Hirsch, T., Gomez-Monterrey, I., Castedo, M., and Kroemer, G. Mitochondrial control of nuclear apoptosis. J. Exp. Med., *183:* 1533–1544, 1996.
40. Bonner, J. A., Vroman, B. T., Christianson, T. J. H., and Karnitz, L. M. Ionizing radiation-induced MEK and ERK activation does not enhance survival of irradiated human squamous carcinoma cells. Int. J. Radiat. Oncol. Biol. Phys., *42:* 921–925, 1998.
41. Irani, K., Xia, Y., Zweier, J. L., Sollot, S. J., Der, C. J., Fearon, E. R., Sundaresan, M., Finkel, T., and Goldschmidt-Clermont, P. J. Mitogenic signaling mediated by oxidants in Ras-transformed fibroblasts. Science (Wash. DC), *275:* 1649–1652, 1997.
42. Rizzuto, R., Pinton, P., Carrington, W., Fay, F., Fogarty, K. E., Lifshitz, L. M., Tuft, R. A., and Pozzan, T. Close contacts with the endoplasmic reticulum as determinants of mitochondrial calcium responses. Science (Wash. DC), *280:* 1763–1766, 1998.
43. Ricken, S., Leipsiger, J., Greger, R., and Nitschke, R. Simultaneous measurements of cytosolic and mitochondrial Ca^{2+} transients in HT29 cells. J. Biol. Chem., *273:* 34961–34969, 1998.
44. Romashko, D. N., Marban, E., and O'Rourke, B. Subcellular metabolic transients and mitochondrial redox waves in heart cells. Proc. Natl. Acad. Sci. USA, *95:* 1618–1623, 1998.
45. Novgorodov, S. A., and Gudz, T. I. Permeability transition pore of the inner mitochondrial membrane can operate in two open states with different selectivities. J. Bioenerg. Biomembr., *28:* 139–146, 1996.
46. Gudz, T., Pandelova, I., and Novgorodov, S. Stimulation of respiration in rat thymocytes induced by ionizing radiation. Radiat. Res., *138:* 114–120, 1994.
47. Okada, S. (ed.). Radiation Biochemistry. New York: Academic Press, 1970.
48. Knebel, A., Rahmsforf, H. J., Ullrich, A., and Herrlich, P. Dephosphorylation of receptor tyrosine kinases as target of regulation by radiation, oxidants, or alkylating agents. EMBO J., *15:* 5314–5325, 1996.
49. Suh, Y. A., Arnold, R. S., Lassegue, B., Shi, J., Xu, X., Sorescu, D., Chung, A. B., Griendling, K. K., and Lambeth, J. D. Cell transformation by the superoxide-generating oxidase Mox1. Nature (Lond.), *401:* 79–82, 1999.
50. Stuehr, D. J. Mammalian nitric oxide synthases. Biochim. Biophys. Acta, *1411:* 217–230, 1999.